

# Chemical gradients in the Milky Way from the RAVE data

## II. Giant stars

C. Boeche<sup>1</sup>, A. Siebert<sup>2</sup>, T. Piffl<sup>3,4</sup>, A. Just<sup>1</sup>, M. Steinmetz<sup>3</sup>, E. K. Grebel<sup>1</sup>, S. Sharma<sup>5</sup>, G. Kordopatis<sup>6</sup>, G. Gilmore<sup>6</sup>, C. Chiappini<sup>3</sup>, K. Freeman<sup>7</sup>, B. K. Gibson<sup>8,9</sup>, U. Munari<sup>10</sup>, A. Siviero<sup>11,3</sup>, O. Bienaymé<sup>2</sup>, J. F. Navarro<sup>12</sup>, Q. A. Parker<sup>13,14,15</sup>, W. Reid<sup>13,15</sup>, G. M. Seabroke<sup>16</sup>, F. G. Watson<sup>14</sup>, R. F. G. Wyse<sup>17</sup>, and T. Zwitter<sup>18</sup>

<sup>1</sup> Astronomisches Rechen-Institut, Zentrum für Astronomie der Universität Heidelberg, Mönchhofstr. 12-14, 69120 Heidelberg, Germany

e-mail: corrado@ari.uni-heidelberg.de

<sup>2</sup> Observatoire astronomique de Strasbourg, Université de Strasbourg, CNRS, UMR 7550, 11 rue de l'Université, 67000 Strasbourg, France

<sup>3</sup> Leibniz Institut für Astrophysik Potsdam (AIP), An der Sternwarte 16, 14482 Potsdam, Germany

<sup>4</sup> Rudolf Peierls Centre for Theoretical Physics, Keble Road, Oxford OX1 3NP, UK

<sup>5</sup> Sydney Institute for Astronomy, School of Physics A28, University of Sydney, Sydney NSW 2006, Australia

<sup>6</sup> Institute of Astronomy, University of Cambridge, Madingley Road, Cambridge CB3 0HA, UK

<sup>7</sup> Research School of Astronomy and Astrophysics, Australian National University, Cotter Rd., ACT 2611 Weston, Australia

<sup>8</sup> Institute for Computational Astrophysics, Dept of Astronomy and Physics, Saint Mary's University, Halifax, NS, BH3 3C3, Canada

<sup>9</sup> Jeremiah Horrocks Institute, University of Central Lancashire, Preston, PR1 2HE, UK

<sup>10</sup> INAF Osservatorio Astronomico di Padova, via dell'Osservatorio 8, 36012 Asiago, Italy

<sup>11</sup> Department of Physics and Astronomy, Padova University, Vicolo dell'Osservatorio 2, 35122 Padova, Italy

<sup>12</sup> Department of Physics and Astronomy, University of Victoria, Victoria, BC, V8P5C2, Canada

<sup>13</sup> Department of Physics and Astronomy, Macquarie University, Sydney, NSW 2109, Australia

<sup>14</sup> Australian Astronomical Observatory, PO Box 915, North Ryde, NSW 1670, Australia

<sup>15</sup> Research Centre for Astronomy, Astrophysics and Astrophotonics, Macquarie University, Sydney, NSW 2109, Australia

<sup>16</sup> Mullard Space Science Laboratory, University College London, Holmbury St Mary, Dorking RH5 6NT, UK

<sup>17</sup> Department of Physics and Astronomy, Johns Hopkins University, 3400 North Charles Street, Baltimore, MD 21218, USA

<sup>18</sup> Faculty of Mathematics and Physics, University of Ljubljana, Jadranska 19, 1000 Ljubljana, Slovenia

Received 10 April 2014 / Accepted 20 June 2014

### ABSTRACT

**Aims.** We provide new constraints on the chemo-dynamical models of the Milky Way by measuring the radial and vertical chemical gradients for the elements Mg, Al, Si, Ti, and Fe in the Galactic disc and the gradient variations as a function of the distance from the Galactic plane ( $Z$ ).

**Methods.** We selected a sample of giant stars from the RAVE database using the gravity criterium  $1.7 < \log g < 2.8$ . We created a RAVE mock sample with the Galaxia code based on the Besançon model and selected a corresponding mock sample to compare the model with the observed data. We measured the radial gradients and the vertical gradients as a function of the distance from the Galactic plane  $Z$  to study their variation across the Galactic disc.

**Results.** The RAVE sample exhibits a negative radial gradient of  $d[\text{Fe}/\text{H}]/dR = -0.054 \text{ dex kpc}^{-1}$  close to the Galactic plane ( $|Z| < 0.4 \text{ kpc}$ ) that becomes flatter for larger  $|Z|$ . Other elements follow the same trend although with some variations from element to element. The mock sample has radial gradients in fair agreement with the observed data. The variation of the gradients with  $Z$  shows that the Fe radial gradient of the RAVE sample has little change in the range  $|Z| \lesssim 0.6 \text{ kpc}$  and then flattens. The iron vertical gradient of the RAVE sample is slightly negative close to the Galactic plane and steepens with  $|Z|$ . The mock sample exhibits an iron vertical gradient that is always steeper than the RAVE sample. The mock sample also shows an excess of metal-poor stars in the  $[\text{Fe}/\text{H}]$  distributions with respect to the observed data. These discrepancies can be reduced by decreasing the number of thick disc stars and increasing their average metallicity in the Besançon model.

**Key words.** Galaxy: abundances – Galaxy: disk – Galaxy: structure – Galaxy: kinematics and dynamics

## 1. Introduction

One of the main structures of the Milky Way is the disc, which, since the work by Gilmore & Reid (1983), has been thought to be composed of two separate components: the thin and the thick disc. These discs are known to vary in their kinematic and chemistry (Freeman & Bland-Hawthorn 2002), therefore they must

have experienced different star formation histories. Recently, the thin-thick disc model has been questioned, since new comprehensive data do not show a clear duality (Ivezić et al. 2008; Bovy et al. 2012). The latest hypothesis suggests that the disc may be one single structure with kinematical and chemical features that are continuously distributed, and that the thin and thick discs can be seen as the two extreme tails of such a structure. A

study of the chemical gradients within the disc has the potential to shed light on its structure and provide important constraints on the formation scenarios of the Galaxy. If star formation in the thick and thin discs occurs independently, it will be detectable through tracing the spatial distribution of chemical abundances with reference to the kinematic structure of the disc.

Several studies were previously undertaken using Cepheids, open clusters, planetary nebulae, and turn-off stars to trace abundances (see references in Boeche et al. 2013, hereafter Paper I). These studies provided radial chemical gradients ranging from  $-0.03$  to  $-0.17$  dex  $\text{kpc}^{-1}$ , and many of them indicate values close to  $\sim -0.05$  dex  $\text{kpc}^{-1}$ . The cause of the fairly large spread among the gradients found by different authors may be because of the different tracers employed. Tracers of different ages represent the chemical evolutionary states of the Galaxy at different times (i.e. at the time when they formed), therefore they can have significantly different gradients. Another reason for the range of the gradient values found in literature may be found in local inhomogeneities because of disrupted open clusters (Montes et al. 2001, and references therein), moving groups generated by resonant features due to spiral arms (Carlberg & Sellwood 1985), the Galactic bar (Minchev & Famaey 2010), or stellar streams due to disrupted Galactic satellites (Belokurov et al. 2006, and reference therein).

All of these causes of inhomogeneity can affect the chemical gradient measurements and make their determination and their interpretation as result of the star formation history of an ideally undisturbed galactic disc more challenging. It is interesting to note how these mechanisms are also employed to explain the kinematical heating of the thin disc or the formation of the thick disc. For instance, Sales et al. (2009) discussed the major mechanisms of thick disc formation, including accretion from disrupted satellites (Abadi et al. 2003) and heating a pre-existing disc by minor mergers (Quinn et al. 1993; Villalobos & Helmi 2008). Kroupa (2002) suggested that the thick disc may be composed of stars formed in star clusters of the early thin disc which, after their evaporation from the clusters, would acquire kinematics that resemble the thick disc. Kinematic heating and radial mixing can also increase the velocity dispersion of a thin disc (Sellwood & Binney 2002; Roškar et al. 2008; Minchev & Famaey 2010, among others). Since these mechanisms are still in action in the present Milky Way, their effects overlap, generating a natural dispersion in the chemical abundance distribution, and making the original causes of the chemical gradients difficult to disentangle. It is worth noting that Balser et al. 2011, by studying H II regions, found differences in radial chemical gradients ranging from  $-0.03$  to  $-0.07$  dex  $\text{kpc}^{-1}$  when measured at different Galactic azimuth, remarking that the abundance distribution in the disc is not only a function of the Galactocentric distance. Therefore, differences in radial chemical gradients of  $\sim 0.04$  dex  $\text{kpc}^{-1}$  between different areas of the disc may occur. If so, precise chemical gradient determinations can reveal inhomogeneities among different regions of the Galaxy, but they may not be decisive in determining the contribution of the different mechanisms to the Galactic disc structure.

Numerous chemical models were developed to match the radial gradients observed. By using different combinations of various ingredients (inside-out formation of the disc, Chiappini et al. 1997, 2001; cosmological hydrodynamical simulations with feedback energy, Gibson et al. 2013; chemodynamical simulation with the smooth particle hydrodynamical method, Kobayashi & Nakasato 2011;  $N$ -body hydrodynamical codes with chemical evolution implemented, Minchev et al. 2013, 2014b; chemical models with radial mixing,

Schönrich & Binney, 2009) the chemical models can cover the range of observed radial gradients cited above (from flatter gradients like  $-0.04$  dex  $\text{kpc}^{-1}$  predicted by the Chiappini et al. 1997 model to the steeper  $-0.11$  dex  $\text{kpc}^{-1}$  of the Schönrich & Binney model).

Thanks to the many spectroscopic surveys undertaken in recent years (the Geneva Copenhagen Survey (GCS), Nordström et al. 2004; the Sloan Extension for Galactic Understanding and Exploration (SEGUE), Yanny et al. 2009; the RADial Velocity Experiment (RAVE), Steinmetz et al. 2006; the *Gaia*-ESO survey, Gilmore et al. 2012; the GALactic Archaeology with HERMES survey (GALAH), Zucker et al. 2012; the Apache Point Observatory Galactic Evolution Experiment survey (APOGEE), Majewski et al. 2010; the Large sky Area Multi-Object fiber Spectroscopic Telescope (LAMOST), Zhao et al. 2012; and soon *Gaia*, Perryman et al. 2001), chemical abundances of a large sample of stars were (and will be) measured for a more comprehensive study of the Milky Way disc in the solar neighborhood and beyond.

In Paper I we undertook a study of the radial chemical gradients in the Milky Way using dwarf stars that were observed and measured in the RAVE survey (Steinmetz et al. 2006) with the more recent stellar parameters, chemical abundances, and distances reported in the Data Release 4 (DR4, Kordopatis et al. 2013). We found a radial [Fe/H] gradient of  $-0.065$  dex  $\text{kpc}^{-1}$  that becomes flatter with increasing distance from the Galactic plane. This is in fair agreement with earlier and later studies (Pasquali & Perinotto 1993; Cheng et al. 2012a; Anders et al. 2014). The comparison with a mock sample created with the Galaxia code (based on the Besançon model, Robin et al. 2003) highlights an excess of moderately low metallicity stars in the mock sample (thick disc stars) with respect to the observed data. Moreover, we found false positive radial metallicity gradients in the  $(R_g, Z_{\text{max}})$  plane ( $R_g$  is the guiding radius and  $Z_{\text{max}}$  the maximum distance that the stars reach along their Galactic orbit) caused by the lack of correlation between the metallicity and the kinematics of the stars in the Galaxia mock sample.

In our present work, we study the radial and vertical gradients of the Galactic disc using giant stars of the RAVE survey. Thanks to their high luminosity, we can probe a large volume above and below the disc, finding similarities but also some differences with respect to the dwarf stars studied in Paper I. The paper is organized as follows: in Sect. 2 we describe the data from which we extract our samples, in Sect. 3 we briefly outline the method, in Sect. 4 we report the analysis and the chemical gradient measured, in Sect. 5 we discuss the results, and we conclude in Sect. 6.

## 2. Data

In the following, we summarize the characteristics of the data, which are the same employed in Paper I (Boeche et al. 2013). Because this sample was selected from the RAVE internal database in 2012, the selection rendered fewer stars than by using the present DR4 database, which contains the complete collection of spectra observed by RAVE. Nonetheless, the radial velocities, stellar parameters, chemical abundances, and distances are the same as the DR4 data release (Kordopatis et al. 2013). The stellar atmospheric parameters, effective temperature  $T_{\text{eff}}$ , gravity  $\log g$ , and metallicity [M/H] are measured by the new RAVE pipeline (Kordopatis et al. 2013) which makes use of the MATrix Inversion for Spectral SynthEsis algorithm (MATISSE; Recio-Blanco et al. 2006) and the DEcision tree alGorithm for ASTrophysics (DEGAS; Bijaoui et al. 2012). Expected errors

at  $S/N \sim 50$  for giant stars are  $\sim 100$  K in  $T_{\text{eff}}$  and  $\sim 0.3$  dex for  $\log g$ . The chemical abundances of the elements Fe, Mg, Al, Si, Ti, and Ni are derived by the RAVE chemical pipeline (Boeche et al. 2011) with some improved features described in Kordopatis et al. (2013). Errors in chemical abundances for  $S/N > 40$  are estimated to be  $\sim 0.10$ – $0.15$  dex for Fe, Mg, Al, and Si,  $\sim 0.2$  dex for Ti, and  $\sim 0.25$  dex for Ni. Proper motions are given as in the DR3 data release (Siebert et al. 2011), i.e. for every star we adopted the proper motion with the smallest error chosen among several catalogues (Tycho2, Høg et al. 2000; the PPM-Extended catalogues PPMX and PPMXL, Roeser et al. 2008, 2010; the Second and Third US Naval Observatory CCD Astrograph Catalog UCAC2 and UCAC3, Zacharias et al. 2004). Proper motion errors vary depending on the catalogue and the source considered. Most of the sources have average errors of  $\sim 4$ – $8$   $\text{mas yr}^{-1}$  (Siebert et al. 2011). Distances are estimated by Binney et al. (2014). Distance errors are estimated to lie between 20% and 40% in linear distance, depending on the spectral class.

With these data we computed absolute positions and velocities of the stars with respect to the Galactic centre. We integrated the Galactic orbits of the stars with the code NEMO (Teuben 1995) adopting the Galactic potential model no 2 by Dehnen & Binney (1998), which assumes  $R_{\odot} = 8.0$  kpc, and best matches the observed properties of the Galaxy. Orbit integration was done for a time of  $40 \text{ Gyr}^1$  to extract information like apocentre  $R_a$ , pericentre  $R_p$ , and maximum distance from the Galactic plane reached by the star along its orbit  $Z_{\text{max}}$ . Using the rotation curve of the Galaxy, we converted the angular momentum into the guiding radius  $R_g$ .

From the RAVE internal database the data sample was selected with the following constraints: i) spectra with  $S/N > 40$ ; ii) for stars with multiple observations we selected only the data from spectra with highest  $S/N$  (to avoid repeated observations of the same object); iii) spectra with high quality flags (Algo\_Conv = 0,  $\chi^2 < 2000$ , frac > 0.7); iv) stars with radial velocity errors smaller than  $8 \text{ km s}^{-1}$ ; v) stars classified as normal stars by Matijević et al. (2012); vi) stars having [Fe/H] estimation. With this selection we are left with 98074 RAVE stars. This sample is the very same sample used in Paper I to study the chemical gradients of the dwarf stars. In this work, we select and study giant stars.

### 2.1. The RAVE giant stars sample

During the analysis of the data we realized that in the RAVE sample selected with the constraints outlined in the previous section, giant stars with  $T_{\text{eff}} < 4250$  K were not included. This is due to the quality criterium Algo\_Conv = 0, which selects only spectra for which the DR4 pipeline code is expected to give more accurate results thanks to the better interpolation between the grid points of the stellar parameter space with MATISSE. At low  $T_{\text{eff}}$ , closer to the grid boundary and where the molecular lines become more and more prominent, the DR4 pipeline favours the DEGAS results over the results of MATISSE. In order to work with homogeneous data we limited our sample to the MATISSE results.

<sup>1</sup> A short integration time such as one or few Gyrs would not suffice to find good approximations of the orbital parameters. The star covers its orbit in the meridian plane after infinite time, therefore, with a long integration time we can better approximate the parameters  $R_a$ ,  $R_p$ , and  $Z_{\text{max}}$  at the present time.

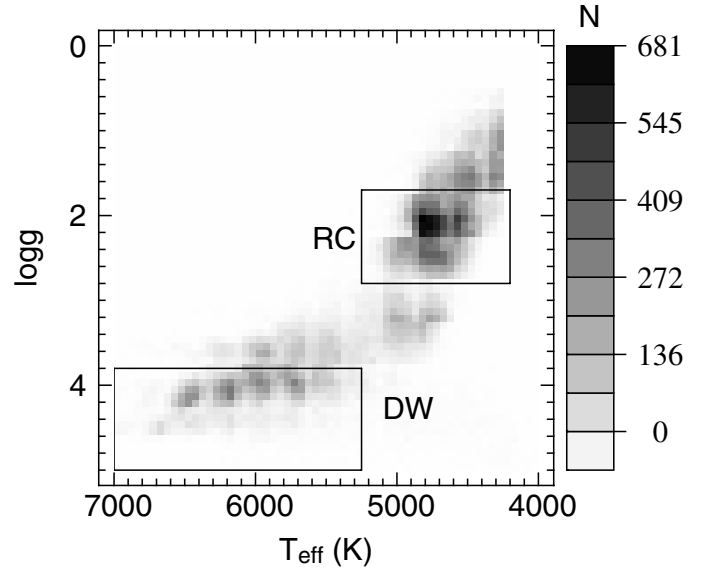


**Fig. 1.** Density distribution of our RAVE sample in the  $(T_{\text{eff}}, \log g)$  plane. The RAVE RC sample as selected by the selection criteria and the dwarf stars sample (DW) as selected in Paper I are reported.

For stars with  $\log g < 1.7$  this temperature cut generates a metallicity bias against high metallicity stars, because their isochrones lie at lower  $T_{\text{eff}}$  with respect to the low metallicity stars. This bias can heavily affect the chemical gradients, therefore we decided to exclude stars with  $\log g < 1.7$  from our analysis. Giant stars with  $\log g > 1.7$  are located at higher  $T_{\text{eff}}$  and they are not affected by this bias (see Fig. 1). We selected our sample as follows: i) effective temperature  $4250 < T_{\text{eff}}(\text{K}) < 5250$ ; ii) gravity  $1.7 < \log g < 2.8$ ; and iii) distance estimation uncertainties smaller than 30%. This selection leaves us with 17 950 stars.

The selection criteria in  $T_{\text{eff}}$  and  $\log g$  are represented by the rectangular set in Fig. 1. Because this is the region of the red clump (RC) stars, we call the sample “the RC sample”. In the same figure we also report the set in  $T_{\text{eff}}$  and  $\log g$  used in Paper I to select the dwarf stars (DW) sample.

### 2.2. The mock sample

In order to avoid possible misinterpretations due to observational biases we used the code Galaxia (Sharma et al. 2011) to create a mock sample to be compared with the RAVE sample. Since Galaxia employs the analytical density profiles of the Besançon model (Robin et al. 2003), the mock sample is a Galaxia realization of the Besançon model but using Padova isochrones (Bertelli et al. 1994; Marigo et al. 2008). We generated a mock sample having the same  $I$  magnitude and colour selections as that of RAVE stars with  $S/N > 40$  and flagged as normal stars by Matijević et al. (2012) (same as in Paper I). Out of the 97 485 stars of this mock RAVE sample, the mock RC sample was selected with the same selection criteria used for the RAVE RC sample outlined in Sect. 2.1. The mock RC sample consists of 33 808 stars. This sample is numerically larger than the RAVE RC sample because the spectrum quality selection criteria (such as Algo\_Conv,  $\chi^2$  and frac parameters) and distance uncertainty criterium are applied to the RAVE sample but not to the mock sample. Like for the DW sample discussed in Paper I, for the RC sample these quality selection criteria are expected to

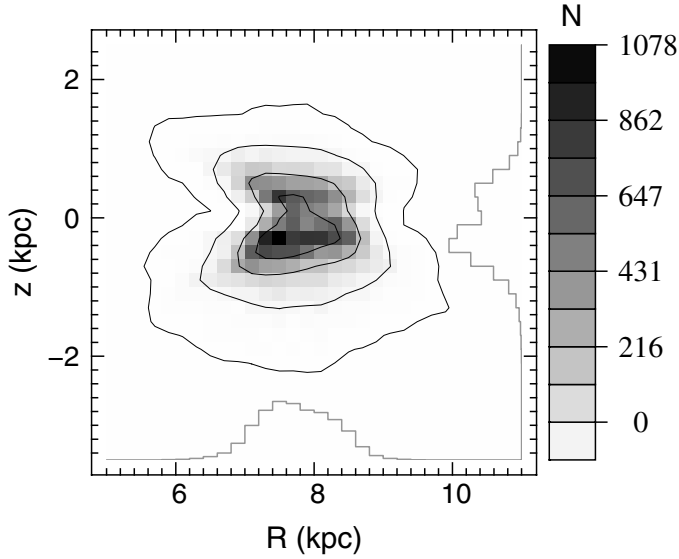


**Fig. 2.** Distribution in  $R$  and  $Z$  for the red clump sample. The grey levels represent the number of stars per bin. The isocontours include 34%, 68%, and 95% of the sample, respectively. The histograms represent the distribution in relative numbers of the stars in  $R$  and  $Z$ .

be independent from the stellar parameters and cause no effects on the chemical gradients.

### 3. Method and error estimation

Here we only summarize the method and error estimations, because they are the very same applied to the DW sample and they are fully discussed in Sect. 3 of Paper I. We measured gradients by fitting the distribution of the stars in the planes  $(R, [\text{Fe}/\text{H}])$  and  $(R_g, [\text{Fe}/\text{H}])$  with a linear regression, and estimated the uncertainties with the bootstrap technique over 1000 realizations. The confidence intervals reported in the paper represent the internal error, because undetected inhomogeneities in the stellar samples (such as disrupted open clusters or stellar streams) can affect the gradients in uncontrolled ways and lead to larger uncertainties. In Paper I, we estimated the external errors to be of the order of  $\sim 0.01$  dex  $\text{kpc}^{-1}$ . The Galactic orbits of the stars of the mock sample and the orbit parameters  $R_g$  and  $Z_{\text{max}}$  were integrated using the same procedure applied for the RAVE stars. The use of kinematics-dependent parameters like  $R_g$  and  $Z_{\text{max}}$  introduces a bias that affects the estimation of the chemical gradients. As discussed in Paper I, stars with small  $R_g$  reach the solar neighbourhood only if they are on eccentric (kinematically hot) orbits. On average, these stars are metal-poorer than stars having the same  $R_g$  and moving on circular orbits, which do not reach the solar neighbourhood, and are therefore missing from the RAVE sample. This generates a bias against metal-rich stars having small  $R_g$ . The bias makes the gradient estimations less negative (or even positive) than they should be, and therefore these are estimations to be taken with great care. In Paper I we had no choice but to use the  $R_g$  and  $Z_{\text{max}}$  parameters because the spatial range in  $R$  and  $Z$  covered by the dwarf stars is too small to permit a robust radial chemical gradient estimate. With the RC stars we can use the  $R$  and  $Z$  parameters because, thanks to their high luminosity, they cover a spatial volume large enough for good chemical gradient estimations (see Fig. 2). Because of the bias that affects the gradient estimations in the  $(R_g, Z_{\text{max}})$  plane, in this work we analysed the  $(R, Z)$  plane and the results

obtained using the  $(R_g, Z_{\text{max}})$  plane are only briefly presented for comparison with Paper I.

#### 3.1. Errors due to spatial distribution and distances

The measured gradients may suffer from some systematics due to the spatial distribution of the RAVE sample. In the  $Z$  bins the stars may be not evenly distributed in  $R$ , leading to gradients that can be more affected by stars located in the inner or outer disc. In the discussion of Sect. 5 we neglected these effects, and our comparisons refer to the mock sample in which the uneven spatial distribution of the stars is reproduced. For the vertical gradients, we measured the gradients in the range  $7.5 < R(\text{kpc}) < 8.5$  to reduce this effect as much as possible.

We also evaluated the impact of the distance errors on the gradients by adding random and systematic errors of 30% in distances to the mock sample. When random errors are applied, we found negligible differences in radial and vertical gradients (smaller than the internal errors), but the vertical gradient at  $0.8 < |Z|(\text{kpc}) < 1.2$  becomes less steep by  $\sim 0.1$  dex  $\text{kpc}^{-1}$ . The systematic errors induce more consistent variations. When inflating (shrinking) the distances by 30% the radial gradients show a negligible difference at  $Z < 0.8$  kpc, but become less (more) positive by  $\sim 0.02$  dex  $\text{kpc}^{-1}$  at  $Z > 0.8$  kpc. The vertical gradients flatten (steepen) by  $\sim 0.1$  dex  $\text{kpc}^{-1}$ .

## 4. Analysis and results

Following the procedure adopted in Paper I, we measured the chemical gradients of the RC sample, dividing it into different sub-samples with different distances  $|Z|$  from the Galactic plane and then investigate how the gradients change with  $Z$ . Unlike the dwarf stars studied in Paper I, the RC sample cover a volume large enough to study the gradients in the  $(R, Z)$  plane at four (instead of three)  $Z$  ranges. The RAVE RC sample stars do not lie beyond  $|Z| = 2.5$  kpc, therefore the chosen  $|Z|$  bins extend up to 2 kpc, which excludes only 2 stars.

We also investigate the difference in chemical gradients of the  $\alpha$ -enhanced stars from the non  $\alpha$ -enhanced stars. The selection criteria of this further subdivision are outlined in Sect. 4.5.

#### 4.1. Radial chemical gradients for the RAVE RC sample

We divided the RAVE RC sample in four sub-samples:  $0.0 < |Z|(\text{kpc}) \leq 0.4$  (named  $Z_{0,0}^{\text{RAVE\_RC}}$  sample),  $0.4 < |Z|(\text{kpc}) \leq 0.8$  (the  $Z_{0,4}^{\text{RAVE\_RC}}$  sample),  $0.8 < |Z|(\text{kpc}) \leq 1.2$  (the  $Z_{0,8}^{\text{RAVE\_RC}}$  sample), and  $1.2 < |Z|(\text{kpc}) < 2.0$  (the  $Z_{1,2}^{\text{RAVE\_RC}}$  sample). We omitted a few outliers located at  $R > 9.5$  kpc and  $R < 4.5$  kpc. With these samples we found that the radial gradients become progressively less negative with  $Z$  (see Fig. 4). For iron the gradients are:

$$\begin{aligned} \frac{d[\text{Fe}/\text{H}]}{dR} Z_{0,0}^{\text{RAVE\_RC}} &= -0.054 \pm 0.004 \text{ dex kpc}^{-1} \text{ (8459 stars);} \\ \frac{d[\text{Fe}/\text{H}]}{dR} Z_{0,4}^{\text{RAVE\_RC}} &= -0.039 \pm 0.004 \text{ dex kpc}^{-1} \text{ (7651 stars);} \\ \frac{d[\text{Fe}/\text{H}]}{dR} Z_{0,8}^{\text{RAVE\_RC}} &= -0.011 \pm 0.008 \text{ dex kpc}^{-1} \text{ (1532 stars); and} \\ \frac{d[\text{Fe}/\text{H}]}{dR} Z_{1,2}^{\text{RAVE\_RC}} &= +0.047 \pm 0.018 \text{ dex kpc}^{-1} \text{ (283 stars).} \end{aligned}$$

We also measured the chemical gradients for the elements Mg, Al, Si, and Ti and their abundance relative to Fe. The results are reported in Tables 1 and 2.

To test the robustness of the results and to compare them with the results in Paper I we also measured the chemical gradients in the  $(R_g, Z_{\text{max}})$  plane. To do so we selected four sub-samples as a function of  $Z_{\text{max}}$  with boundaries of  $0.0 < Z_{\text{max}}(\text{kpc}) \leq 0.4$ ,

**Table 1.** Radial abundance gradients measured in the RC RAVE sample for Fe, Mg, Al, Si, and Ti expressed as dex kpc<sup>-1</sup> for four ranges of  $|Z|$ .

	$\frac{d[\text{Fe}/\text{H}]}{dR}$	$\frac{d[\text{Mg}/\text{H}]}{dR}$	$\frac{d[\text{Al}/\text{H}]}{dR}$	$\frac{d[\text{Si}/\text{H}]}{dR}$	$\frac{d[\text{Ti}/\text{H}]}{dR}$	$\frac{d[\text{Fe}/\text{H}]}{dR}$ (mock)
$0.0 <  Z  \text{ (kpc)} \leq 0.4$	$-0.054 \pm 0.004$	$-0.034 \pm 0.004$	$-0.035 \pm 0.005$	$-0.064 \pm 0.005$	$+0.008 \pm 0.004$	$-0.049 \pm 0.006$
$0.4 <  Z  \text{ (kpc)} \leq 0.8$	$-0.039 \pm 0.004$	$-0.031 \pm 0.004$	$-0.032 \pm 0.005$	$-0.046 \pm 0.004$	$-0.005 \pm 0.003$	$-0.019 \pm 0.005$
$0.8 <  Z  \text{ (kpc)} \leq 1.2$	$-0.011 \pm 0.008$	$-0.023 \pm 0.007$	$-0.027 \pm 0.009$	$-0.028 \pm 0.008$	$-0.015 \pm 0.006$	$+0.030 \pm 0.009$
$1.2 <  Z  \text{ (kpc)} < 2.0$	$+0.047 \pm 0.018$	$+0.025 \pm 0.015$	$+0.060 \pm 0.022$	$+0.009 \pm 0.018$	$+0.032 \pm 0.017$	$+0.061 \pm 0.012$

**Notes.** For comparison, in the last column, the vertical  $[\text{Fe}/\text{H}]$  gradients of the mock sample are reported. Uncertainties of 68% confidence are obtained with the bootstrap method and represent the internal errors.

**Table 2.** As Table 1, but for relative abundances  $[X/\text{Fe}]$ .

	$\frac{d[\text{Mg}/\text{Fe}]}{dR}$	$\frac{d[\text{Al}/\text{Fe}]}{dR}$	$\frac{d[\text{Si}/\text{Fe}]}{dR}$	$\frac{d[\text{Ti}/\text{Fe}]}{dR}$
$0.0 <  Z  \text{ (kpc)} \leq 0.4$	$+0.020 \pm 0.004$	$+0.019 \pm 0.004$	$-0.009 \pm 0.003$	$+0.063 \pm 0.003$
$0.4 <  Z  \text{ (kpc)} \leq 0.8$	$+0.009 \pm 0.004$	$+0.006 \pm 0.004$	$-0.006 \pm 0.003$	$+0.035 \pm 0.003$
$0.8 <  Z  \text{ (kpc)} \leq 1.2$	$-0.012 \pm 0.008$	$-0.015 \pm 0.008$	$-0.017 \pm 0.006$	$-0.002 \pm 0.006$
$1.2 <  Z  \text{ (kpc)} < 2.0$	$-0.022 \pm 0.018$	$+0.009 \pm 0.019$	$-0.037 \pm 0.012$	$-0.013 \pm 0.013$

$0.4 < Z_{\text{max}} \text{ (kpc)} \leq 0.8$ ,  $0.8 < Z_{\text{max}} \text{ (kpc)} \leq 1.2$ , and  $1.2 < Z_{\text{max}} \text{ (kpc)} \leq 10.0$  and we found iron gradients of  $d[\text{Fe}/\text{H}]/dR_g = -0.029 \pm 0.003$ ,  $-0.014 \pm 0.002$ ,  $+0.000 \pm 0.003$ , and  $0.029 \pm 0.003$  dex kpc<sup>-1</sup>, respectively. The flatter gradients are due to the bias discussed in Sect. 3.

#### 4.2. Radial chemical gradients for the mock RC samples

By applying the same cuts in  $Z$  seen before, for the mock RC sample the Fe radial gradients are (see Fig. 5):

$$\begin{aligned} \frac{d[\text{Fe}/\text{H}]}{dR} Z_{0.0}^{\text{mock\_RC}} &= -0.049 \pm 0.005 \text{ dex kpc}^{-1} \text{ (15 524 stars);} \\ \frac{d[\text{Fe}/\text{H}]}{dR} Z_{0.4}^{\text{mock\_RC}} &= -0.019 \pm 0.005 \text{ dex kpc}^{-1} \text{ (13 304 stars);} \\ \frac{d[\text{Fe}/\text{H}]}{dR} Z_{0.8}^{\text{mock\_RC}} &= +0.030 \pm 0.009 \text{ dex kpc}^{-1} \text{ (3599 stars); and} \\ \frac{d[\text{Fe}/\text{H}]}{dR} Z_{1.2}^{\text{mock\_RC}} &= +0.061 \pm 0.012 \text{ dex kpc}^{-1} \text{ (1189 stars).} \end{aligned}$$

For the mock sample there are no other elements for which we can measure the gradients because the model provides only iron abundance. We measured the gradients for the mock RC sample in the  $(R_g, Z_{\text{max}})$  plane and we found that they are always positive, similar to what we found in Paper I for dwarf stars. For the intervals  $0.0 < Z_{\text{max}} \text{ (kpc)} \leq 0.4$ ,  $0.4 < Z_{\text{max}} \text{ (kpc)} \leq 0.8$ ,  $0.8 < Z_{\text{max}} \text{ (kpc)} \leq 1.2$ , and  $1.2 < Z_{\text{max}} \text{ (kpc)} \leq 10.0$  the iron gradients for the RC mock sample are  $d[\text{Fe}/\text{H}]/dR_g = +0.051 \pm 0.003$ ,  $+0.057 \pm 0.002$ ,  $+0.068 \pm 0.004$ , and  $+0.064 \pm 0.007$  dex kpc<sup>-1</sup>. The comparison with the RAVE RC sample is discussed in Sect. 5.2.

#### 4.3. Vertical chemical gradients for the RAVE RC sample

The RAVE vertical gradients are not constant but exhibit variations as a function of  $Z$ . We investigate these variations by following the continuous abundances variation along  $Z$  (see Sect. 4.6) and by measuring them in four  $Z$  intervals (the same intervals as employed for the radial gradients). Because the RAVE stars cover a volume that is roughly (non-symmetric) cone-shaped, their  $R$  distribution depends on their  $Z$ . This can affect the estimation of the vertical gradient because the average abundances at a given  $Z$  may refer to different  $R$ . To limit this bias as much as possible, we measured the vertical gradients at  $R \sim 8$  kpc by considering only stars within the interval

$7.5 \leq R \text{ (kpc)} < 8.5$ . We summarize here the vertical gradients for the iron abundance of the RAVE RC sample:

$$\begin{aligned} \frac{d[\text{Fe}/\text{H}]}{dZ} Z_{0.0}^{\text{RAVE\_RC}} &= -0.050 \pm 0.027 \text{ dex kpc}^{-1} \text{ (5903 stars);} \\ \frac{d[\text{Fe}/\text{H}]}{dZ} Z_{0.4}^{\text{RAVE\_RC}} &= -0.087 \pm 0.030 \text{ dex kpc}^{-1} \text{ (3815 stars);} \\ \frac{d[\text{Fe}/\text{H}]}{dZ} Z_{0.8}^{\text{RAVE\_RC}} &= -0.148 \pm 0.073 \text{ dex kpc}^{-1} \text{ (661 stars); and} \\ \frac{d[\text{Fe}/\text{H}]}{dZ} Z_{1.2}^{\text{RAVE\_RC}} &= -0.199 \pm 0.070 \text{ dex kpc}^{-1} \text{ (129 stars).} \end{aligned}$$

When the iron vertical gradient is measured over the whole sample in the  $0.0 < |Z| < 2.0$  kpc range, it amounts to  $\frac{d[\text{Fe}/\text{H}]}{dZ} = -0.112 \pm 0.007$  dex kpc<sup>-1</sup> (10 511 stars). The vertical gradients for the individual elements are reported in Table 3.

#### 4.4. Vertical chemical gradients for the mock RC sample

For the mock sample we repeated the same procedure used to measure the vertical gradient of the RAVE RC sample. They are significantly steeper than in the observational data, and they are:

$$\begin{aligned} \frac{d[\text{Fe}/\text{H}]}{dZ} Z_{0.0}^{\text{mock\_RC}} &= -0.373 \pm 0.031 \text{ dex kpc}^{-1} \text{ (10 776 stars);} \\ \frac{d[\text{Fe}/\text{H}]}{dZ} Z_{0.4}^{\text{mock\_RC}} &= -0.409 \pm 0.038 \text{ dex kpc}^{-1} \text{ (6224 stars);} \\ \frac{d[\text{Fe}/\text{H}]}{dZ} Z_{0.8}^{\text{mock\_RC}} &= -0.536 \pm 0.085 \text{ dex kpc}^{-1} \text{ (1440 stars); and} \\ \frac{d[\text{Fe}/\text{H}]}{dZ} Z_{1.2}^{\text{mock\_RC}} &= -0.338 \pm 0.083 \text{ dex kpc}^{-1} \text{ (471 stars).} \end{aligned}$$

When the vertical gradient is measured over the whole sample in the  $0.0 < |Z| < 2.0$  kpc range, this is  $\frac{d[\text{Fe}/\text{H}]}{dZ} = -0.400 \pm 0.008$  dex kpc<sup>-1</sup> (18 919 stars). For comparison this is also reported in Table 3.

#### 4.5. Chemical gradients of the $\alpha$ -poor and $\alpha$ -rich stars

Thin- and thick-disc stars (as usually defined in the frame of the thin- thick-disc dichotomy) chemically differ from their enhancement in  $\alpha$  elements with respect to iron. Recently, some authors (Schlesinger et al. 2014; Hayden et al. 2014; Lee et al. 2011; Cheng et al. 2012b) analyzed their samples by dividing them in  $\alpha$ -enhanced and non  $\alpha$ -enhanced stars in the attempt to highlight their different behaviour. For comparison purposes we follow their example and divide the RAVE RC sample as a function of the magnesium enhancement with respect to iron  $[\text{Mg}/\text{Fe}]$ . The use of other  $\alpha$  elements like Si or Ti is

**Table 3.** Vertical abundance gradients measured in the RC RAVE sample for Fe, Mg, Al, Si, and Ti expressed as dex kpc<sup>-1</sup> for four ranges of  $|Z|$ .

	$\frac{d[\text{Fe}/\text{H}]}{dZ}$	$\frac{d[\text{Mg}/\text{H}]}{dZ}$	$\frac{d[\text{Al}/\text{H}]}{dZ}$	$\frac{d[\text{Si}/\text{H}]}{dZ}$	$\frac{d[\text{Ti}/\text{H}]}{dZ}$	$\frac{d[\text{Fe}/\text{H}]}{dZ}$ (mock)
$0.0 <  Z  \text{ (kpc)} \leq 0.4$	$-0.050 \pm 0.027$	$+0.019 \pm 0.022$	$+0.045 \pm 0.030$	$-0.088 \pm 0.030$	$+0.081 \pm 0.023$	$-0.373 \pm 0.031$
$0.4 <  Z  \text{ (kpc)} \leq 0.8$	$-0.087 \pm 0.030$	$+0.022 \pm 0.025$	$-0.027 \pm 0.034$	$-0.117 \pm 0.033$	$+0.076 \pm 0.023$	$-0.409 \pm 0.038$
$0.8 <  Z  \text{ (kpc)} \leq 1.2$	$-0.148 \pm 0.073$	$-0.031 \pm 0.061$	$-0.124 \pm 0.075$	$-0.197 \pm 0.078$	$+0.010 \pm 0.055$	$-0.536 \pm 0.085$
$1.2 <  Z  \text{ (kpc)} < 2.0$	$-0.199 \pm 0.070$	$+0.041 \pm 0.096$	$+0.031 \pm 0.104$	$-0.140 \pm 0.096$	$-0.086 \pm 0.068$	$-0.338 \pm 0.083$

**Notes.** For comparison, in the last column, the vertical  $[\text{Fe}/\text{H}]$  gradients of the mock sample are reported. Only stars in the range  $7.5 \leq R(\text{kpc}) < 8.5$  are considered. Uncertainties of 68% confidence are obtained with the bootstrap method and represent the internal errors.

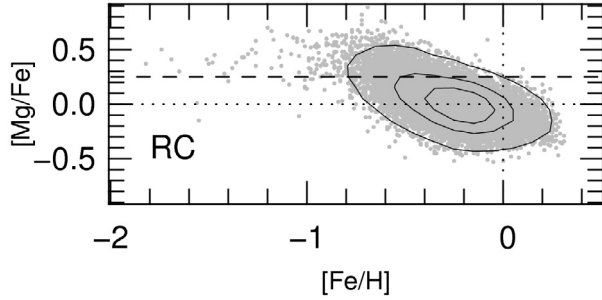


**Fig. 3.** Distribution of the RAVE RC stars in the  $([\text{Fe}/\text{H}], [\text{Mg}/\text{Fe}])$  plane. The isocountours holds 34%, 68%, and 95% of the stars. The dashed line at  $[\text{Mg}/\text{Fe}] = +0.25$  dex separate the  $\alpha$ -rich stars (above the line) from the  $\alpha$ -poor stars (below the line).

not appropriate because their behaviour looks peculiar (this is reported in Sect. 5.1). Because we do not see bimodality in the chemistry distribution of the RAVE sample (see Fig. 3) we made few attempts to separate these two sub-samples by cutting at  $[\text{Mg}/\text{Fe}] = 0.15, 0.20,$  and  $0.25$  dex. We noticed that for progressively higher  $[\text{Mg}/\text{Fe}]$  the  $\alpha$ -enhanced sample can be distinguished from the non  $\alpha$ -enhanced sample for the different gradients, although the smaller size of the  $\alpha$ -enhanced sample obtained with higher  $[\text{Mg}/\text{Fe}]$  cuts delivers a poorer statistic. To emphasize this difference in gradients, we decided to cut at  $[\text{Mg}/\text{Fe}] = 0.25$  dex and we call  $\alpha$ -rich those stars with  $[\text{Mg}/\text{Fe}] > 0.25$  dex and  $\alpha$ -poor those with  $[\text{Mg}/\text{Fe}] \leq 0.25$  dex. With this further sub-division we perform the radial and vertical gradients measurements with the same procedure used in the previous sections. Here we briefly summarize the results for iron.

The iron radial gradients for the  $\alpha$ -poor stars are:

$$\begin{aligned} \frac{d[\text{Fe}/\text{H}]}{dR} Z_{0.0}^{\text{RAVE\_RC}} &= -0.054 \pm 0.004 \text{ dex kpc}^{-1} \text{ (7971 stars);} \\ \frac{d[\text{Fe}/\text{H}]}{dR} Z_{0.4}^{\text{RAVE\_RC}} &= -0.045 \pm 0.004 \text{ dex kpc}^{-1} \text{ (6874 stars);} \\ \frac{d[\text{Fe}/\text{H}]}{dR} Z_{0.8}^{\text{RAVE\_RC}} &= -0.026 \pm 0.008 \text{ dex kpc}^{-1} \text{ (1256 stars); and} \\ \frac{d[\text{Fe}/\text{H}]}{dR} Z_{1.2}^{\text{RAVE\_RC}} &= +0.040 \pm 0.019 \text{ dex kpc}^{-1} \text{ (197 stars),} \end{aligned}$$

while for the  $\alpha$ -rich stars they are:

$$\begin{aligned} \frac{d[\text{Fe}/\text{H}]}{dR} Z_{0.0}^{\text{RAVE\_RC}} &= -0.010 \pm 0.018 \text{ dex kpc}^{-1} \text{ (488 stars);} \\ \frac{d[\text{Fe}/\text{H}]}{dR} Z_{0.4}^{\text{RAVE\_RC}} &= +0.009 \pm 0.011 \text{ dex kpc}^{-1} \text{ (777);} \\ \frac{d[\text{Fe}/\text{H}]}{dR} Z_{0.8}^{\text{RAVE\_RC}} &= -0.002 \pm 0.014 \text{ dex kpc}^{-1} \text{ (276 stars); and} \\ \frac{d[\text{Fe}/\text{H}]}{dR} Z_{1.2}^{\text{RAVE\_RC}} &= +0.047 \pm 0.028 \text{ dex kpc}^{-1} \text{ (86 stars).} \end{aligned}$$

The iron vertical gradients for the  $\alpha$ -poor stars are:

$$\begin{aligned} \frac{d[\text{Fe}/\text{H}]}{dZ} Z_{0.0}^{\text{RAVE\_RC}} &= +0.004 \pm 0.025 \text{ dex kpc}^{-1} \text{ (5566 stars);} \\ \frac{d[\text{Fe}/\text{H}]}{dZ} Z_{0.4}^{\text{RAVE\_RC}} &= -0.028 \pm 0.028 \text{ dex kpc}^{-1} \text{ (3461 stars);} \\ \frac{d[\text{Fe}/\text{H}]}{dZ} Z_{0.8}^{\text{RAVE\_RC}} &= -0.085 \pm 0.076 \text{ dex kpc}^{-1} \text{ (546 stars); and} \\ \frac{d[\text{Fe}/\text{H}]}{dZ} Z_{1.2}^{\text{RAVE\_RC}} &= -0.141 \pm 0.090 \text{ dex kpc}^{-1} \text{ (87 stars).} \end{aligned}$$

The vertical gradient measured over the whole  $\alpha$ -poor sample in the  $0.0 < |Z| < 2.0$  kpc range is  $\frac{d[\text{Fe}/\text{H}]}{dZ} = -0.067 \pm 0.008$  dex kpc<sup>-1</sup> (9663 stars).

For the  $\alpha$ -rich stars, the vertical gradients are:

$$\begin{aligned} \frac{d[\text{Fe}/\text{H}]}{dZ} Z_{0.0}^{\text{RAVE\_RC}} &= -0.312 \pm 0.113 \text{ dex kpc}^{-1} \text{ (337 stars);} \\ \frac{d[\text{Fe}/\text{H}]}{dZ} Z_{0.4}^{\text{RAVE\_RC}} &= +0.015 \pm 0.092 \text{ dex kpc}^{-1} \text{ (354 stars);} \\ \frac{d[\text{Fe}/\text{H}]}{dZ} Z_{0.8}^{\text{RAVE\_RC}} &= +0.141 \pm 0.120 \text{ dex kpc}^{-1} \text{ (115 stars); and} \\ \frac{d[\text{Fe}/\text{H}]}{dZ} Z_{1.2}^{\text{RAVE\_RC}} &= -0.073 \pm 0.088 \text{ dex kpc}^{-1} \text{ (42 stars).} \end{aligned}$$

The vertical gradient measured over the whole  $\alpha$ -rich sample in the  $0.0 < |Z| < 2.0$  kpc range is  $\frac{d[\text{Fe}/\text{H}]}{dZ} = -0.021 \pm 0.017$  dex kpc<sup>-1</sup> (848 stars). The results for the other elements are reported in Tables 4 and 5.

#### 4.6. Gradient estimates with moving box car

Here we want to investigate how the radial chemical gradients change with  $Z$ . We select sub-samples of stars that lie in an interval 0.2 kpc wide and, starting from  $Z = -2.0$  kpc, we shift this interval of 0.2 kpc each step up to  $Z = +2.0$  kpc and measure the gradient  $d[X/\text{H}]/dR$  at every step. We impose the condition that the interval must contain no less than 1000 stars. If the interval contains less than 1000 stars the interval width increases until this number is reached, with a width maximum limit of 0.6 kpc. We avoid the interval between  $Z = \pm 0.1$  kpc because of the small range in  $R$  covered by the RAVE sample in this region, and because of its scarcity of points. This procedure was applied to the five RAVE element abundances of the RAVE RC sample, and to the iron abundance of the mock RC sample. For the RAVE sample this procedure was also applied to the abundances relative to iron  $[X/\text{Fe}]$ . We also want to see how the median abundances and abundances relative to iron change with  $Z$  (i.e., the vertical gradients). We repeated the same procedure by measuring the median abundance of the stars contained in a  $Z$  interval 0.2 kpc wide and moving the interval in 0.2 kpc steps from  $Z = -2.0$  kpc to  $Z = +2.0$  kpc. Here we imposed a lower limit of 20 stars per interval. If this limit is not reached, the interval width is increased up to a maximum of 0.6 kpc. The results for the RAVE and the mock RC samples are illustrated in Fig. 6 to Fig. 9.

## 5. Discussion

The comparison between the RAVE RC sample and the mock RC sample in the  $(R_g, Z_{\text{max}})$  plane brings us to the same consideration reported in Paper I for the dwarfs stars sample: when kinematical parameters like  $R_g$  and  $Z_{\text{max}}$  are used to estimate the radial gradients, the mock sample yields unrealistic positive gradients because the Fe abundances of the stars in the model are assigned as a function of their spatial position, disregarding their kinematics. As a consequence, the thin disc stars (which

**Table 4.** Radial abundance gradients for Fe, Mg, Al, Si, and Ti elements measured for the RC RAVE sample divided in  $\alpha$ -poor (top) and  $\alpha$ -rich (bottom) sub-samples.

	$\frac{d[\text{Fe}/\text{H}]}{dR}$	$\frac{d[\text{Mg}/\text{H}]}{dR}$	$\frac{d[\text{Al}/\text{H}]}{dR}$	$\frac{d[\text{Si}/\text{H}]}{dR}$	$\frac{d[\text{Ti}/\text{H}]}{dR}$
$\alpha$ -poor sample					
$0.0 <  Z  \text{ (kpc)} \leq 0.4$	$-0.054 \pm 0.004$	$-0.037 \pm 0.004$	$-0.036 \pm 0.005$	$-0.065 \pm 0.005$	$+0.009 \pm 0.004$
$0.4 <  Z  \text{ (kpc)} \leq 0.8$	$-0.045 \pm 0.004$	$-0.035 \pm 0.004$	$-0.041 \pm 0.005$	$-0.050 \pm 0.005$	$-0.008 \pm 0.003$
$0.8 <  Z  \text{ (kpc)} \leq 1.2$	$-0.026 \pm 0.008$	$-0.020 \pm 0.007$	$-0.031 \pm 0.010$	$-0.039 \pm 0.009$	$-0.018 \pm 0.007$
$1.2 <  Z  \text{ (kpc)} < 2.0$	$+0.040 \pm 0.019$	$+0.030 \pm 0.016$	$+0.049 \pm 0.025$	$+0.004 \pm 0.020$	$+0.035 \pm 0.016$
$\alpha$ -rich sample					
$0.0 <  Z  \text{ (kpc)} \leq 0.4$	$-0.010 \pm 0.018$	$-0.001 \pm 0.017$	$+0.016 \pm 0.023$	$-0.003 \pm 0.019$	$+0.021 \pm 0.019$
$0.4 <  Z  \text{ (kpc)} \leq 0.8$	$+0.009 \pm 0.011$	$+0.001 \pm 0.011$	$+0.028 \pm 0.014$	$-0.010 \pm 0.011$	$+0.026 \pm 0.011$
$0.8 <  Z  \text{ (kpc)} \leq 1.2$	$-0.002 \pm 0.014$	$-0.018 \pm 0.014$	$-0.041 \pm 0.019$	$-0.022 \pm 0.015$	$-0.018 \pm 0.014$
$1.2 <  Z  \text{ (kpc)} < 2.0$	$+0.047 \pm 0.028$	$+0.026 \pm 0.031$	$+0.085 \pm 0.043$	$+0.009 \pm 0.026$	$+0.019 \pm 0.039$

**Notes.** The gradients are expressed as dex  $\text{kpc}^{-1}$  for four ranges of  $|Z|$ . Uncertainties of 68% confidence are obtained with the bootstrap method and represent the internal errors.

**Table 5.** Vertical abundance gradients for Fe, Mg, Al, Si, and Ti elements measured for the RC RAVE sample divided in  $\alpha$ -poor (top) and  $\alpha$ -rich (bottom) sub-samples.

	$\frac{d[\text{Fe}/\text{H}]}{dZ}$	$\frac{d[\text{Mg}/\text{H}]}{dZ}$	$\frac{d[\text{Al}/\text{H}]}{dZ}$	$\frac{d[\text{Si}/\text{H}]}{dZ}$	$\frac{d[\text{Ti}/\text{H}]}{dZ}$
$\alpha$ -poor sample					
$0.0 <  Z  \text{ (kpc)} \leq 0.4$	$+0.004 \pm 0.025$	$+0.025 \pm 0.023$	$+0.071 \pm 0.029$	$-0.048 \pm 0.030$	$+0.095 \pm 0.023$
$0.4 <  Z  \text{ (kpc)} \leq 0.8$	$-0.028 \pm 0.028$	$+0.009 \pm 0.026$	$+0.004 \pm 0.033$	$-0.083 \pm 0.033$	$+0.103 \pm 0.024$
$0.8 <  Z  \text{ (kpc)} \leq 1.2$	$-0.085 \pm 0.076$	$-0.131 \pm 0.064$	$-0.061 \pm 0.081$	$-0.153 \pm 0.086$	$+0.029 \pm 0.062$
$1.2 <  Z  \text{ (kpc)} < 2.0$	$-0.141 \pm 0.090$	$-0.084 \pm 0.098$	$+0.108 \pm 0.143$	$-0.066 \pm 0.120$	$-0.121 \pm 0.085$
$\alpha$ -rich sample					
$0.0 <  Z  \text{ (kpc)} \leq 0.4$	$-0.312 \pm 0.113$	$-0.189 \pm 0.114$	$-0.051 \pm 0.134$	$-0.243 \pm 0.111$	$+0.077 \pm 0.129$
$0.4 <  Z  \text{ (kpc)} \leq 0.8$	$+0.015 \pm 0.092$	$-0.004 \pm 0.089$	$+0.004 \pm 0.115$	$+0.061 \pm 0.094$	$+0.062 \pm 0.104$
$0.8 <  Z  \text{ (kpc)} \leq 1.2$	$+0.141 \pm 0.120$	$+0.192 \pm 0.112$	$-0.077 \pm 0.174$	$+0.071 \pm 0.144$	$+0.133 \pm 0.125$
$1.2 <  Z  \text{ (kpc)} < 2.0$	$-0.073 \pm 0.088$	$-0.016 \pm 0.108$	$+0.015 \pm 0.130$	$-0.094 \pm 0.150$	$+0.072 \pm 0.131$

**Notes.** Only stars in the range  $7.5 \leq R \text{ (kpc)} < 8.5$  are considered. The gradients are expressed as dex  $\text{kpc}^{-1}$  for four ranges of  $|Z|$ . Uncertainties of 68% confidence are obtained with the bootstrap method and represent the internal errors.

have a radial gradient of  $d[\text{Fe}/\text{H}]/dR = -0.07 \text{ dex kpc}^{-1}$  in the Besançon model) have zero gradient in the  $(R_g, [\text{Fe}/\text{H}])$  plane because their position in  $R$  is re-distributed in  $R_g$  independent of their metallicity. On the other hand, the thick disc stars (which are metal poorer and have more eccentric orbits with respect to the thin disc stars) lie to the lower-left corner of the  $(R_g, [\text{Fe}/\text{H}])$  plane. Thin and thick disc stars together generate an apparent positive gradient that is not real. Such a bias is also visible in real data with a flattening of the gradients, as we saw for the dwarf stars in Sect. 6.1 of Paper I. Therefore, in the following we mainly discuss the gradients in the  $(R, [\text{Fe}/\text{H}])$  plane.

At the beginning of our analysis, we divided the  $|Z|$  ranges into four bins. Because the Galactic disc is expected to be roughly symmetric with respect to  $Z = 0$ , the choice of bins in  $|Z|$  increases the number of stars per bin and makes the statistic more robust. Nonetheless, we decided to study at higher resolution how the gradient changes with  $Z$  by using smaller bins of 0.2 kpc width. The two analyses are consistent with each other and the higher resolution allows us to determine if (and where) possible transitions occur in the vertical structure of the disc.

### 5.1. Chemical gradients of the RAVE RC sample

Tables 1 to 5 hold a considerable amount of information that is not always straightforward to interpret. In the following we avoid discussing every chemical gradient measured, and we focus only on the main outcomes of our measurements. A detailed comparison with models (necessary to fully understand all the

reported gradients) is left to a future work. Here we summarize the main results for the RAVE RC sample:

- the radial gradients are negative and become progressively flatter with growing  $|Z|$ ;
- vertical gradients are negative and become progressively steeper with growing  $|Z|$ ;
- the negative radial gradients observed are driven by the  $\alpha$ -poor stars, while the  $\alpha$ -rich stars have radial gradients consistent with zero;
- the vertical gradients of the  $\alpha$ -poor stars are consistent with zero for  $|Z| < 0.8 \text{ kpc}$  and are slightly negative beyond 0.8 kpc;
- the vertical gradients of the  $\alpha$ -rich stars are negative for  $|Z| < 0.4 \text{ kpc}$  and consistent with zero for  $|Z| > 0.4 \text{ kpc}$ ;
- the radial gradients of the abundances relative to iron have small positive or zero values up to  $|Z| \sim 0.8 \text{ kpc}$  and then become negative.

These results have general validity, although a closer look at the gradient values reveals that there are differences between the elements, and that some elements behave alike. In fact, Si behaves like Fe, Al behaves like Mg, and Ti behaves differently from all the others. The similar behaviour of Si and Fe is unexpected, since Si is an  $\alpha$  element and it should behave like Mg. The peculiar behaviour of Ti is equally singular. A future detailed comparison with chemo-dynamical models will help to address the reasons behind such differences and similarities.

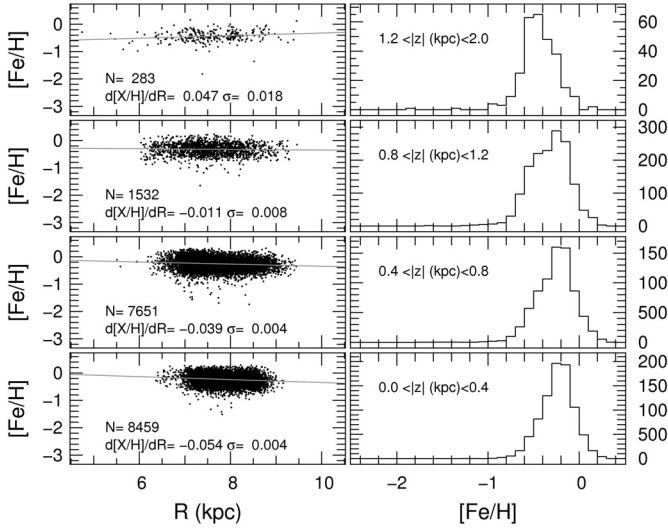


**Fig. 4.** Distribution of the RAVE RC sample at different  $Z$  intervals in the  $(R, [\text{Fe}/\text{H}])$  plane (*left panels*) and metallicity distributions (*right panels*).

In the proximity of the Galactic plane ( $|Z| < 0.4$  kpc) the  $\alpha$ -poor and  $\alpha$ -rich samples have a remarkable behaviour. The chemistry and spatial location of the  $\alpha$ -poor stars would identify them as thin disc stars and we would expect that they would drive the vertical gradient at  $|Z| < 0.4$  kpc. Unlike the expectations, their iron vertical gradient is consistent with zero ( $+0.004 \pm 0.025$  dex  $\text{kpc}^{-1}$ ) and this is in striking contrast with the mock sample ( $-0.373 \pm 0.031$  dex  $\text{kpc}^{-1}$ ). This suggests a moderate chemical vertical homogeneity in the proximity of the Galactic disc and it may be a sign of weak correlation between metallicity and vertical velocity dispersion.

On the other hand, the  $\alpha$ -rich stars at  $|Z| < 0.4$  (which we would identify as thick disc stars close to the Galactic plane) exhibit a negative iron vertical gradient ( $-0.312 \pm 0.113$  dex  $\text{kpc}^{-1}$ ), revealing a correlation between metallicity and distance from the Galactic plane at small  $Z$ . This reflects the result of Minchev et al. (2014a) who, using RAVE data, found that the vertical velocity dispersion of the giant stars increases with  $[\text{Mg}/\text{Fe}]$  and suddenly decreases for  $[\text{Mg}/\text{Fe}] \gtrsim 0.4$  dex. These high Mg-enhanced stars clump close to the Galactic plane and, according to Minchev et al. (2014a), they would have migrated from the inner disc as result of massive mergers in the early history of the Galaxy.

## 5.2. Comparison between the RAVE and the mock RC samples

At  $|Z| < 0.4$  kpc the mock RC sample exhibits an iron radial gradient in good agreement with the RAVE RC sample and, for both samples, the iron radial gradient becomes flatter with  $|Z|$  (see Table 1, Figs. 4 and 5). For the stars at larger  $|Z|$ , the radial iron gradient becomes positive for both the RAVE and the mock samples. This positive gradient may be due to the spatial distribution of the RAVE stars and not to an intrinsic positive radial gradient of the disc at that  $|Z|$  range. Significant differences between the RAVE RC sample and the mock RC sample can be found in the vertical gradients. The iron vertical gradients in the mock RC sample are much steeper than in the RAVE sample (see Table 3 and Fig. 7). We explain this by comparing the right panels of Figs. 4 and 5. While for the RAVE RC sample the mode of the  $[\text{Fe}/\text{H}]$  distribution moves from  $[\text{Fe}/\text{H}] \sim -0.2$  dex

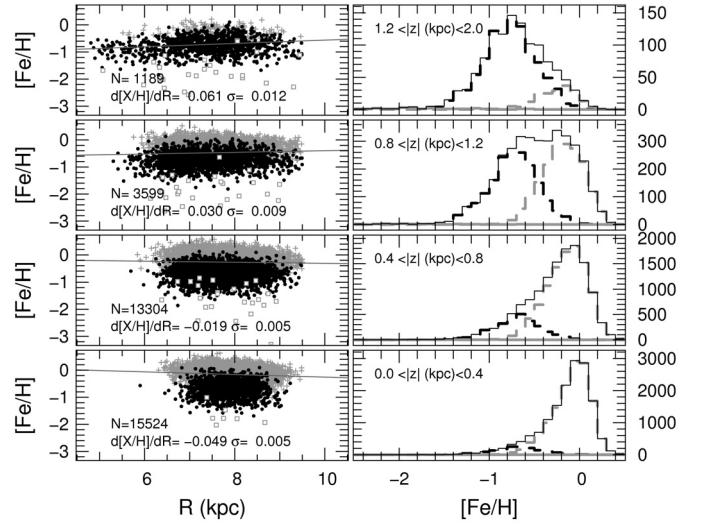


**Fig. 5.** As in Fig. 4, but for the mock sample. Grey plus symbols, black points and grey squares represent thin, thick, and halo stars.

to  $[\text{Fe}/\text{H}] \sim -0.5$  dex in the range  $0.0 < |Z|$  (kpc)  $< 2.0$ , for the mock RC sample the mode of the  $[\text{Fe}/\text{H}]$  distribution spans  $\sim 0.8$  dex in the same  $|Z|$  range. The grey and black dashed histograms in the right panels of Fig. 5 (representing the thick- and thin-disc stars, respectively) clearly show that the shift of the  $[\text{Fe}/\text{H}]$  mode is due to the thick-disc that takes over the thin-disc with growing  $|Z|$ . This means that the steep vertical metallicity observed in the mock RC sample is caused by the overlap of the thin- and the thick-disc, which have different average metallicities and scale heights. The difference in average metallicity of the two discs also explains the broader  $[\text{Fe}/\text{H}]$  distribution of the RC mock sample with respect to the RAVE RC sample. This interpretation is also supported by the analysis of the  $\alpha$ -poor and  $\alpha$ -rich samples. The iron vertical gradients of the  $\alpha$ -poor and the  $\alpha$ -rich samples are consistent with zero or slightly negative values<sup>2</sup>. This suggests that the vertical gradients seen in the RAVE RC sample can also be explained by the superposition of two populations with zero or shallow vertical gradients having different metallicities and scale heights: one with small scale-height and metal-rich and the other with large scale-height and metal poor.

The mock RC sample would find a better agreement with the RAVE data if the average metallicity of the model's thick-disc was shifted from  $-0.78$  dex to  $\sim -0.5$  dex.

## 5.3. Comparison with other observational works

The negative radial gradients that become shallower as we move away from the Galactic plane are in fair agreement (within the external errors,  $\sim 0.01$  dex  $\text{kpc}^{-1}$ ) with the results obtained with the DW sample in Paper I, although the values are not exactly comparable because for the DW sample we measured the radial gradients in the  $(R_g, Z_{\text{max}})$  plane while here we considered the  $(R, Z)$  plane<sup>3</sup>.

<sup>2</sup> The negative values have low significance, because they are consistent with zero inside  $1-2\sigma$  (Table 5). Here we also neglect the negative value shown by the  $\alpha$ -rich sample at  $|Z| < 0.4$ , which we discussed in the previous section.

<sup>3</sup> When the  $(R_g, Z_{\text{max}})$  plane is considered, the RC sample shows shallower radial gradients but the trend is the same (i.e. the gradients are shallower when the distance from the Galactic plane increases).

A similar conclusion can be drawn by considering the work of Anders et al. (2014) for their radial gradients measured on the  $(R_{\text{med}}, Z_{\text{max}})$  plane with APOGEE stars ( $R_{\text{med}}$  is the median radius of the Galactic orbit). When the  $(R, Z)$  plane is used, the gradients of Anders et al. are in good agreement with the RAVE results, except for  $|z| < 0.4$  kpc, where the gradient is steeper than the RAVE gradient.

Hayden et al. (2014), also employing APOGEE stars, found negative inner- and outer-disc radial gradients, flatter for the former, steeper for the latter. The gradients become flatter with  $Z$  and the break between the inner- and outer-disc gradients progressively shifts to larger  $R$ . Although in the RAVE RC sample we do not see any break, our radial gradients have values that seem to lie between the inner- and outer-disc gradients found by Hayden et al., and they flatten with  $Z$  in the same manner as Hayden's gradients.

Significant differences are found for the  $\alpha$ -poor and  $\alpha$ -rich samples. In the Hayden et al. sample both  $\alpha$ -poor and  $\alpha$ -rich stars exhibit negative radial gradients, while in our RAVE sample only the  $\alpha$ -poor stars exhibit negative radial gradients, while the radial gradients of the RAVE  $\alpha$ -rich stars are consistent with zero. The vertical gradients found by Hayden et al. are significantly more negative ( $\sim -0.31$ ,  $-0.21$  and  $-0.26$  dex  $\text{kpc}^{-1}$  at  $7 < R(\text{kpc}) < 9$  for their whole sample,  $\alpha$ -poor sample, and  $\alpha$ -rich sample, respectively) with respect to the RAVE RC sample ( $\sim -0.11$ ,  $-0.067$  and  $-0.021$  dex  $\text{kpc}^{-1}$  for the whole RAVE RC sample,  $\alpha$ -poor sample, and  $\alpha$ -rich sample, respectively) in the  $0 < |Z| (\text{kpc}) < 2$  range.

The radial gradients of the SEGUE sample studied by Cheng et al. (2012b) agree with our results with negative and zero radial gradients for the  $\alpha$ -poor and the  $\alpha$ -rich stars, respectively, although the  $\alpha$ -poor stars of the SEGUE sample at  $|Z| < 0.5$  kpc are steeper than the RAVE sample ( $-0.1$  versus  $-0.05$  dex  $\text{kpc}^{-1}$ ). In the framework of the thin-/thick-disc dichotomy, the zero radial gradients exhibited by the  $\alpha$ -rich stars agree with other previous works in which the authors claimed no detectable radial gradient in the thick disc (Coşkunoğlu et al. 2012 by using RAVE DR3 data; Ruchti et al. 2011; Cheng et al. 2012a).

In the SEGUE sample studied by Schlesinger et al. (2014) the vertical gradient at the solar circle is  $-0.243^{+0.039}_{-0.053}$  dex  $\text{kpc}^{-1}$  in the range  $0.5 \lesssim |Z|(\text{kpc}) \lesssim 1.7$ . For comparison purposes we measured the iron vertical gradient of our RAVE RC sample in the same  $|Z|$  range obtaining  $-0.159 \pm 0.016$  dex  $\text{kpc}^{-1}$ , which may be consistent with the Schlesinger et al. gradient inside a  $2\sigma$  error. The SEGUE  $\alpha$ -poor stars show a positive vertical metallicity gradient ( $+0.063^{+0.047}_{-0.032}$  dex  $\text{kpc}^{-1}$ ), which might be consistent (inside a  $2\sigma$  error) with our zero or negative gradient for  $|Z| > 0.4$  kpc. The vertical gradient of the SEGUE  $\alpha$ -rich stars ( $+0.038^{+0.043}_{-0.037}$  dex  $\text{kpc}^{-1}$ ) is consistent with our results. Unfortunately, they have no results for  $|Z| < 0.4$  kpc to be compared with our zero and negative gradients of the  $\alpha$ -poor and  $\alpha$ -rich stars, respectively.

While the absence of a radial gradient in the thick disc seems to be confirmed by different studies, the vertical gradient is still debated. Some studies found no significant vertical gradients in the thick disc (Allende Prieto et al. 2006; Peng et al. 2013), whereas others claim negative vertical gradients (Bilir et al. 2012 by using RAVE DR3 data; Chen et al. 2011; Ruchti et al. 2011; Katz et al. 2011). Our work suggest that the vertical gradient of the thick disc may be consistent with zero.

#### 5.4. Comparison with models

We stressed before that a detailed comparison of our observational results with Galaxy models is beyond the scope of this work. Nonetheless, in Sect. 5.2 we compared our results with the mock sample (which is a Galaxia realization of the Besançon 2003 model) and here we would like very briefly to compare our results with a few chemical and chemo-dynamical models found in the literature as a first check.

Great care must be taken in drawing conclusions when comparing results from different sources. Observational data, as much as results from chemical or chemo-dynamical models, may refer to samples of stars having different age distribution, therefore referring to different evolutionary phases of the Galaxy. Chemical simulations of the Galaxy showed that stars of different ages can have significantly different radial gradients (Minchev et al. 2013, 2014b; Schönrich & Binney 2009), therefore a sample of stars covering a wide range of ages can exhibit gradients that are a function of their age distribution. Our RAVE RC sample covers presumably a wide range of ages but we do not know its exact age distribution. Keeping this uncertainty in mind, we report here some results from chemical and chemo-dynamical models.

In the  $|Z| \lesssim 0.4$  kpc range (Table 1), our iron radial gradient is in qualitative agreement with the predictions of chemical evolution models of the Galaxy, which assume an inside-out formation process of the disc (Chiappini et al. 2001; Cescutti et al. 2007; Gibson et al. 2013). The predicted gradients of the Cescutti et al. (2007) model for Fe and Mg ( $-0.052$  dex  $\text{kpc}^{-1}$  and  $-0.039$  dex  $\text{kpc}^{-1}$ , respectively) are particularly close to our findings, whereas for Si ( $-0.035$  dex  $\text{kpc}^{-1}$ ) the gradient is too flat with respect to our  $-0.064$  dex  $\text{kpc}^{-1}$  reported in Table 1. The predicted Ti ( $-0.032$  dex  $\text{kpc}^{-1}$ ) does not agree with our zero radial gradient found for this element. The metallicity gradients of  $\sim -0.05$  dex  $\text{kpc}^{-1}$  predicted by the models of Minchev et al. (2014a,b) for moderately young stars (age  $< 4$  Gyr) can be in reasonable agreement with our RC sample. The model by Schönrich & Binney (2009) predicts a metallicity gradient ( $-0.11$  dex  $\text{kpc}^{-1}$ ) too steep with respect to our results.

#### 5.5. On the constancy of the chemical gradients

We estimate the gradients by fitting the data with linear laws, which is convenient for a rough estimate but it may oversimplify the reality. In the evolution of a galaxy, stochastic processes may play a significant role (e.g. where and when an open cluster is going to burst, or a disrupted satellite is accreted by the Galaxy), generating coarse distributions of the stars in velocity and chemical space. Irregularity in the distributions can be revealed only by accurate measurements. When accurate chemical abundances are available, the distributions of the stars in the  $(R, [X/H])$  and  $(Z, [X/H])$  planes are clearly not linear. Hayden et al. (2014) subdivide the radial metallicity gradient observed with the APOGEE data into two linear laws; Balser et al. (2011) found different radial gradients when they are measured at different Galactic azimuth; by using SEGUE data Schlesinger et al. 2014 show clear wiggles in the iron abundance as a function of  $Z$ . Haywood et al. (2013) suggested that the negative radial gradients measured may be the result of the superposition of an inner and an outer disc, which have different average metallicities and  $\alpha$ -enhancement because they experienced different star formation histories. In this scenario, the radial metallicity gradient would not be linear but step-like. Thanks to the large

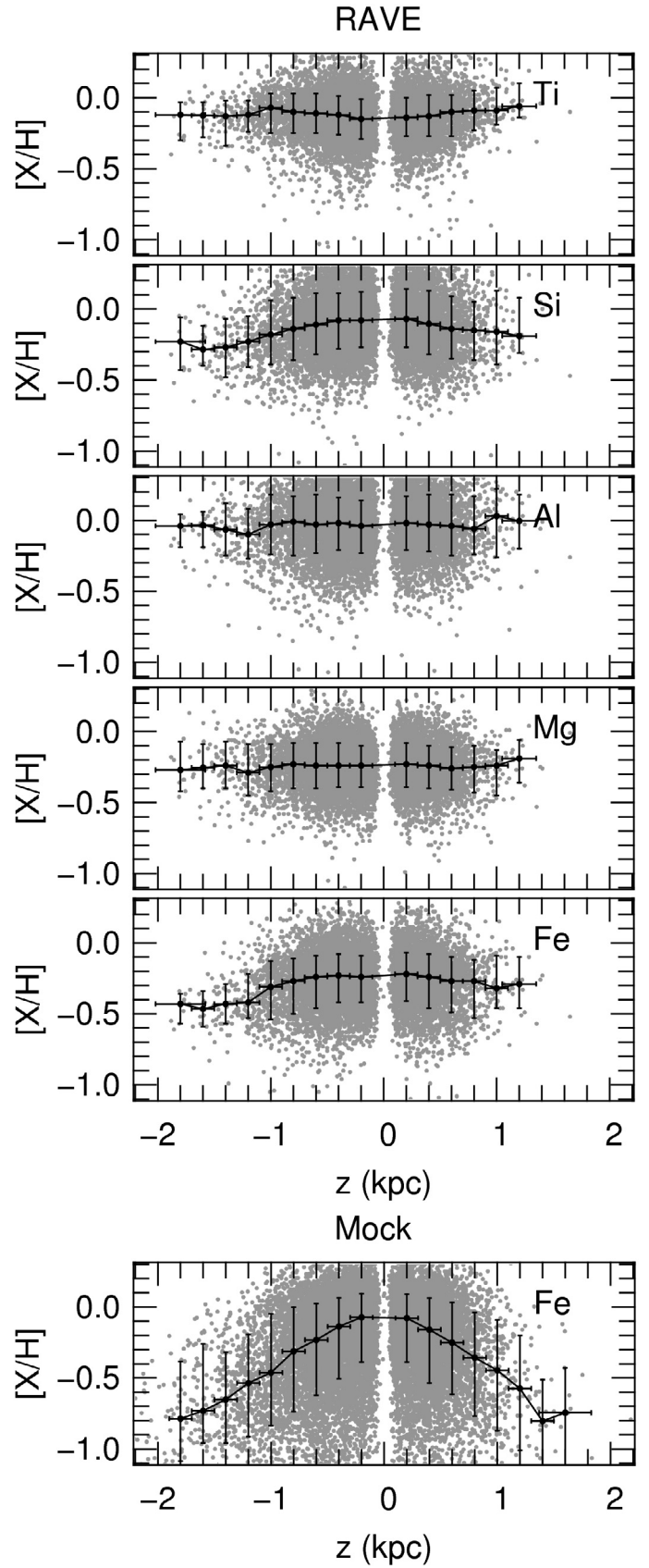
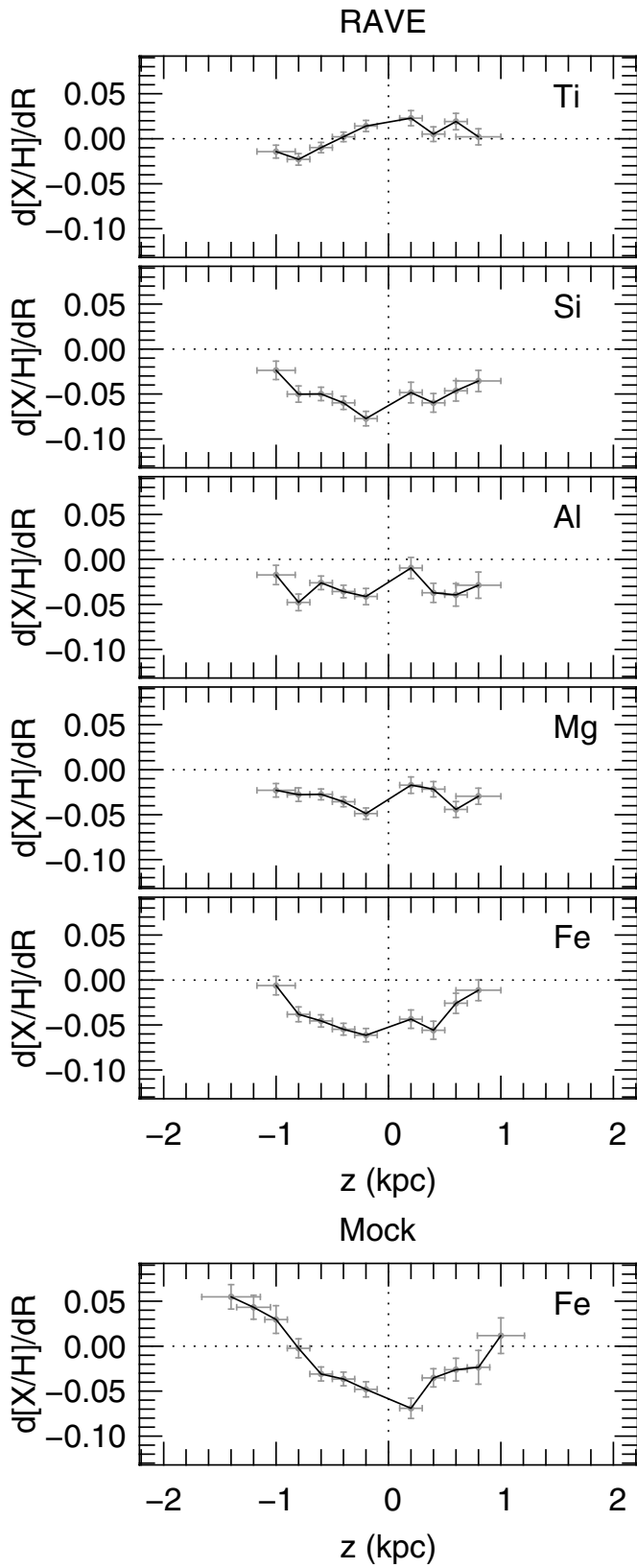


**Fig. 6.** Radial gradients for the RAVE RC sample (*top panels*) and the RC mock sample (*bottom panel*) as a function of the distance from the Galactic plane  $Z$ . The horizontal bars represent the  $Z$  interval taken to measure the gradient  $d[X/H]/dR$ , while the vertical bars represent the uncertainty (68% confidence) of the gradient estimates.

**Fig. 7.** Abundances of the RAVE RC sample (*top panels*) and RC mock sample (*bottom panel*) as a function of  $Z$  in the range  $7.5 < R$  (kpc)  $< 8.5$ . The black points represent the median abundance of the samples in step of 0.2 kpc, while the vertical bars contain 68% of the stars in the bin.

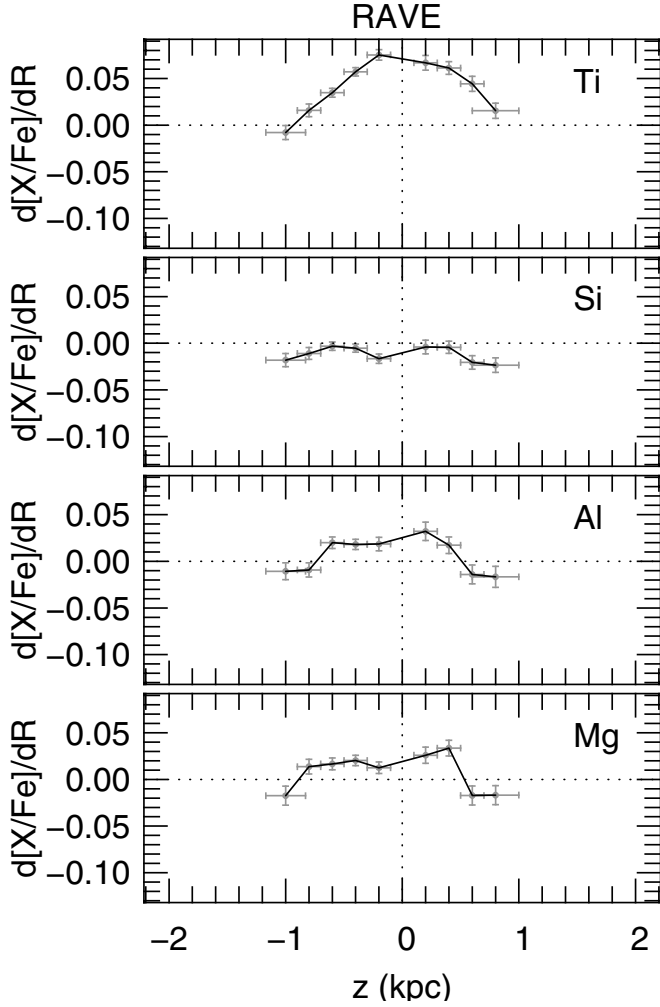


Fig. 8. As in Fig. 6 but for the elemental abundance ratio  $[X/Fe]$ .

amount of data expected from the coming big spectroscopic surveys (such as *Gaia*, Perryman et al. 2001; GALAH, Zucker et al. 2012; 4MOST, de Jong et al. 2012, among others) it will be possible to perform “tomographies” of the disc, and move from 1D to 3D in the analysis of the chemical gradients.

## 6. Conclusions

In this work, we measured the radial and vertical chemical abundance gradients of the Galactic disc in the range  $4.5 < R(\text{kpc}) < 9.5$  for the elements Mg, Al, Si, Ti, and Fe to provide new constraints to the chemical Galactic models. We selected a sample of 17 950 giant stars (the RAVE RC sample) from the RAVE internal database on the basis of the gravity values in the range  $1.7 < \log g < 2.8$ . Similarly, we selected a corresponding sample of stars from a mock RAVE sample created with the Galaxia code (Sharma et al. 2011) and based on the Besançon model (Robin et al. 2003) to compare our data with a well-established Galaxy model. The RAVE and the mock samples are the same samples used in our previous paper (Boeche et al. 2013, Paper I) in which we studied the radial gradients by means of dwarf stars. We divided the RAVE and mock RC samples in four consecutive  $|Z|$  bins with boundaries at 0, 0.4, 0.8, 1.2, and 2 kpc to study the radial gradients as a function of  $Z$  for the five elements under analysis. For a deeper analysis, we further subdivided the

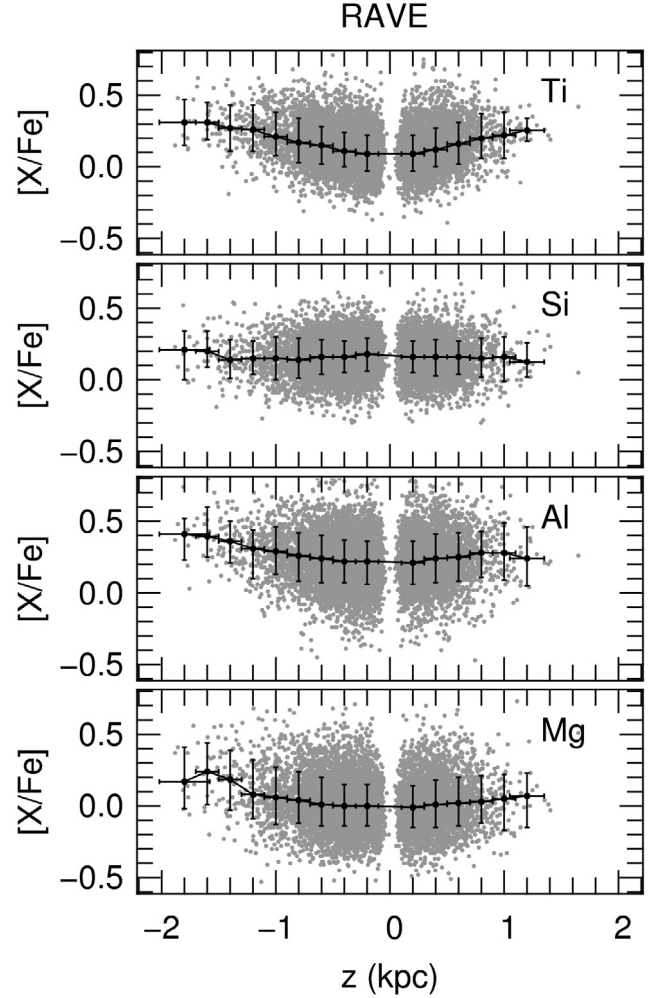


Fig. 9. As in Fig. 7 but for the elemental abundance ratio  $[X/Fe]$ .

samples in  $\alpha$ -poor ( $[Mg/Fe] \lesssim 0.25$  dex) and  $\alpha$ -rich ( $[Mg/Fe] > 0.25$  dex) stars. Our major results can be summarized with the following points:

- the radial chemical gradients are negative and become progressively flatter with  $|Z|$ ;
- the vertical chemical gradients are negative and become progressively steeper with  $|Z|$  (but seem to flat out at large  $|Z|$ );
- the  $\alpha$ -rich stars have radial chemical gradients consistent with zero;
- the vertical chemical gradients of the  $\alpha$ -poor stars are consistent with zero or with being slightly negative;
- the vertical chemical gradients of the  $\alpha$ -rich stars are consistent with zero but close to the Galactic plane, where they are negative.

These results are generally valid although there can be differences depending on the element and the  $|Z|$  interval considered. To fully address the reasons of these differences a detailed comparison with Galactic chemical models is needed.

Close to the Galactic disc the RAVE RC sample has a  $[Fe/H]$  radial gradient of  $-0.055$  dex  $\text{kpc}^{-1}$ , and it becomes flatter with  $|Z|$ . This is in good agreement with previous works (Boeche et al. 2013; Cheng et al. 2012a; Hayden et al. 2014; Anders et al. 2014). This is also in agreement with the mock RC sample, which can reproduce the radial gradient as well as its

flattening with  $|Z|$ . By studying the RAVE RC sample as a function of the  $\alpha$ -enhancement, we found that the  $\alpha$ -poor stars drive the radial gradients while the  $\alpha$ -rich stars show radial gradients consistent with zero. In the framework of the thin/thick disc duality, this suggests that the thick disc may have no radial gradient. This supports the results of previous studies (Coşkunoğlu et al. 2012; Ruchti et al. 2011; Cheng et al. 2012a,b).

The vertical chemical gradients exhibited by the RAVE RC sample are negative ( $-0.11$  dex  $\text{kpc}^{-1}$ ) but shallower than the mock RC sample ( $-0.40$  dex  $\text{kpc}^{-1}$ ). The steep gradient exhibited by the mock RC sample originates from the difference in average metallicity (0.78 dex) between the thin- and the thick-disc stars combined with their different scale-heights. The same difference in average metallicity also explains the broader metallicity distribution of the mock RC sample with respect to the RAVE RC sample. These discrepancies can be reduced by increasing the average  $[\text{Fe}/\text{H}]$  of the thick disc in the mock RC sample from the actual  $[\text{Fe}/\text{H}] = -0.78$  dex to  $\sim -0.5$  dex, as suggested in Boeche et al. (2013) and supported by other studies (Soubiran et al. 2003; Ivezić et al. 2008; Kordopatis et al. 2011). The proposed explanation of the negative vertical gradient as a result of the overlap of two populations with shallow or no vertical gradient (as the thin- and thick-disc in the mock RC sample) finds support in the study of the vertical gradient of the RAVE  $\alpha$ -poor and  $\alpha$ -rich samples. The individual vertical gradients of these two samples are consistent with zero or being slightly negative. Therefore, similarly to the mock RC sample and in the framework of the thin- thick-disc duality, the negative vertical gradient observed in the RAVE RC sample could be mainly caused by the superposition of two populations, one having high metallicity and small scale-height and the other having low metallicity and large scale-height.

The vertical iron gradient observed in the RAVE RC sample seems slightly flatter than found by Schlesinger et al. (2014) and definitely flatter than found by Hayden et al. (2014). We found that the  $\alpha$ -rich sample has a significant negative  $[\text{Fe}/\text{H}]$  vertical gradient at  $|Z| < 0.4$ . This is consistent with the work by Minchev et al. (2014a) who, by using RAVE data, found an unexpected small vertical velocity dispersion for stars with  $[\text{Mg}/\text{Fe}] \geq 0.4$  dex, suggesting radial migration of stars from the inner disc as result of massive mergers in the early history of the Galaxy.

Our current knowledge of the Galactic disc tells us that it cannot be homogeneous and that a unique radial (or vertical) chemical gradient value cannot be valid for the whole disc. Our work and other studies (Schlesinger et al. 2014; Hayden et al. 2014; Balsa et al. 2011), show that the chemical gradients can vary vertically and radially as well as in Galactic azimuth, and that the linear laws used to describe the change of chemical abundances through the Galactic disc seem to be an oversimplification. Future large spectroscopic surveys like the *Gaia*-ESO survey (Gilmore et al. 2012), the GALactic Archaeology with HERMES survey (GALAH; Zucker et al. 2012), the Apache Point Observatory Galactic Evolution Experiment survey (APOGEE; Majewski et al. 2010), the Large sky Area Multi-Object fiber Spectroscopic Telescope (LAMOST; Zhao et al. 2012), and *Gaia* (Perryman et al. 2001) will be able to bring new information about the spatial and chemical distribution of the Galactic disc, and will permit us to perform a “tomography” of the disc, disentangling the spatial chemical distribution due to the Galactic disc formation from the expected inhomogeneities due to moving groups, disrupted open clusters, and stellar streams due to merging Galactic satellites.

**Acknowledgements.** We thank the anonymous referee for the constructive comments that helped to improve the paper. B.C. thanks J. Rybizki the useful discussions during the preparation of this work. We acknowledge funding from Sonderforschungsbereich SFB 881 “The Milky Way System” (subproject A5) of the German Research Foundation (DFG). Funding for RAVE has been provided by the Australian Astronomical Observatory; the Leibniz-Institut fuer Astrophysik Potsdam (AIP); the Australian National University; the Australian Research Council; the French National Research Agency; the German Research Foundation (SPP 1177 and SFB 881); the European Research Council (ERC-StG 240271 Galactica); the Istituto Nazionale di Astrofisica at Padova; The Johns Hopkins University; the National Science Foundation of the USA (AST-0908326); the W. M. Keck foundation; the Macquarie University; the Netherlands Research School for Astronomy; the Natural Sciences and Engineering Research Council of Canada; the Slovenian Research Agency; the Swiss National Science Foundation; the Science & Technology Facilities Council of the UK; Opticon; Strasbourg Observatory; and the Universities of Groningen, Heidelberg and Sydney. The RAVE web site is at <http://www.rave-survey.org>.

## References

- Abadi, M. G., Navarro, J. F., Steinmetz, M., & Eke, V. R. 2003, *ApJ*, 597, 21  
 Allende Prieto, C., Beers, T. C., Wilhelm, R., et al. 2006, *ApJ*, 636, 804  
 Anders, F., Chiappini, C., Santiago, B. X., et al. 2014, *A&A*, 564, A115  
 Balsa, D. S., Rood, R. T., Bania, T. M., & Anderson, L. D. 2011, *ApJ*, 738, 27  
 Belokurov, V., Zucker, D. B., Evans, N. W., et al. 2006, *ApJ*, 642, L137  
 Bertelli, G., Bressan, A., Chiosi, C., Fagotto, F., & Nasi, E. 1994, *A&AS*, 106, 275  
 Bijaoui, A., Recio-Blanco, A., de Laverny, P., et al. 2012, *Statistic. Methodol.*, 9, 55  
 Bilir, S., Karaali, S., Ak, S., et al. 2012, *MNRAS*, 421, 3362  
 Binney, J., Burnett, B., Kordopatis, G., et al. 2014, *MNRAS*, 437, 351  
 Boeche, C., Siebert, A., Williams, M., et al. 2011, *AJ*, 142, 193  
 Boeche, C., Siebert, A., Piffl, T., et al. 2013, *A&A*, 559, A59  
 Bovy, J., Rix, H.-W., & Hogg, D. W. 2012, *ApJ*, 751, 131  
 Brunetti, M., Chiappini, C., & Pfenninger, D. 2011, *A&A*, 534, A75  
 Carlberg, R. G., & Sellwood, J. A. 1985, *ApJ*, 292, 79  
 Cescutti, G., Matteucci, F., François, P., & Chiappini, C. 2007, *A&A*, 462, 943  
 Chen, Y. Q., Zhao, G., Carrell, K., & Zhao, J. K. 2011, *AJ*, 142, 184  
 Cheng, J. Y., Rockosi, C. M., Morrison, H. L., et al. 2012a, *ApJ*, 746, 149  
 Cheng, J. Y., Rockosi, C. M., Morrison, H. L., et al. 2012b, *ApJ*, 752, 51  
 Chiappini, C., Matteucci, F., & Gratton, R. 1997, *ApJ*, 477, 765  
 Chiappini, C., Matteucci, F., & Romano, D. 2001, *ApJ*, 554, 1044  
 Coşkunoğlu, B., Ak, S., Bilir, S., et al. 2012, *MNRAS*, 419, 2844  
 Dehnen, W., & Binney, J. 1998, *MNRAS*, 294, 429  
 de Jong, R. S., Bellido-Tirado, O., Chiappini, C., et al. 2012, *Proc. SPIE*, 8446  
 Freeman, K., & Bland-Hawthorn, J. 2002, *ARA&A*, 40, 487  
 Friel, E. D., Janes, K. A., Tavares, M., et al. 2002, *AJ*, 124, 2693  
 Gibson, B. K., Pilkington, K., Brook, C. B., Stinson, G. S., & Bailin, J. 2013, *A&A*, 554, A47  
 Gilmore, G., & Reid, N. 1983, *MNRAS*, 202, 1025  
 Gilmore, G., Randich, S., Asplund, M., et al. 2012, *The Messenger*, 147, 25  
 Hayden, M. R., Holtzman, J. A., Bovy, J., et al. 2014, *AJ*, 147, 116  
 Haywood, M., Di Matteo, P., Lehnert, M. D., Katz, D., & Gómez, A. 2013, *A&A*, 560, A109  
 Høg, E., Fabricius, C., Makarov, V. V., et al. 2000, *A&A*, 355, L27  
 Ivezić, Ž., Sesar, B., Jurić, M., et al. 2008, *ApJ*, 684, 287  
 Katz, D., Soubiran, C., Cayrel, R., et al. 2011, *A&A*, 525, A90  
 Kobayashi, C., & Nakasato, N. 2011, *ApJ*, 729, 16  
 Kordopatis, G., Recio-Blanco, A., de Laverny, P., et al. 2011, *A&A*, 535, A107  
 Kordopatis, G., Gilmore, G., Steinmetz, M., et al. 2013, *AJ*, 146, 134  
 Kroupa, P. 2002, *MNRAS*, 330, 707  
 Lee, Y. S., Beers, T. C., An, D., et al. 2011, *ApJ*, 738, 187  
 Luck, R. E., Kovtyukh, V. V., & Andrievsky, S. M. 2006, *AJ*, 132, 902  
 Majewski, S. R., Wilson, J. C., Hearty, F., Schiavon, R. R., & Skrutskie, M. F. 2010, *IAU Symp.*, 265, 480  
 Marigo, P., Girardi, L., Bressan, A., et al. 2008, *A&A*, 482, 883  
 Matijević, G., Zwitter, T., Bienaymé, O., et al. 2012, *ApJS*, 200, 14  
 Minchev, I., & Famaey, B. 2010, *ApJ*, 722, 112  
 Minchev, I., Famaey, B., Combes, F., et al. 2011, *A&A*, 527, A147  
 Minchev, I., Chiappini, C., & Martig, M. 2013, *A&A*, 558, A9  
 Minchev, I., Chiappini, C., Martig, M., et al. 2014a, *ApJ*, 781, L20  
 Minchev, I., Chiappini, C., & Martig, M. 2014b, *A&A*, submitted [[arXiv:1401.5796](https://arxiv.org/abs/1401.5796)]  
 Montes, D., López-Santiago, J., Gálvez, M. C., et al. 2001, *MNRAS*, 328, 45  
 Nordström, B., Mayor, M., Andersen, J., et al. 2004, *A&A* 418, 989  
 Pasquali, A., & Perinotto, M. 1993, *A&A*, 280, 581

- Peng, X., Du, C., Wu, Z., Ma, J., & Zhou, X. 2013, *MNRAS*, 434, 3165
- Perryman, M. A. C., de Boer, K. S., Gilmore, G., et al. 2001, *A&A*, 369, 339
- Quinn, P. J., Hernquist, L., & Fullagar, D. P. 1993, *ApJ*, 403, 74
- Recio-Blanco, A., Bijaoui, A., & de Laverny, P. 2006, *MNRAS*, 370, 141
- Robin, A. C., Reylé, C., Derrière, S., & Picaud, S. 2003, *A&A*, 409, 523
- Röser, S., Schilbach, E., Schwan, H., et al. 2008, *A&A*, 488, 401
- Roeser, S., Demleitner, M., & Schilbach, E. 2010, *AJ*, 139, 2440
- Roškar, R., Debattista, V. P., Quinn, T. R., Stinson, G. S., & Wadsley, J. 2008, *ApJ*, 684, L79
- Ruchti, G. R., Fulbright, J. P., Wyse, R. F. G., et al. 2011, *ApJ*, 737, 9
- Sales, L. V., Helmi, A., Abadi, M. G., et al. 2009, *MNRAS*, 400, L61
- Schlesinger, K. J., Johnson, J. A., Rockosi, C. M., et al. 2014, *ApJ*, submitted [[arXiv:1405.6724](https://arxiv.org/abs/1405.6724)]
- Schönrich, R., & Binney, J. 2009, *MNRAS*, 396, 203
- Sellwood, J. A., & Binney, J. J. 2002, *MNRAS*, 336, 785
- Sharma, S., Bland-Hawthorn, J., Johnston, K. V., & Binney, J. 2011, *ApJ*, 730, 3
- Siebert, A., Williams, M. E. K., Siviero, A., et al. 2011, *AJ*, 141, 187
- Soubiran, C., Bienaymé, O., & Siebert, A. 2003, *A&A*, 398, 141
- Steinmetz, M., Zwitter, T., Siebert, A., et al. 2006, *AJ*, 132, 1645
- Teuben, P. J. 1995, in *Astronomical Data Analysis Software and Systems IV*, eds. R. Shaw, H. E. Payne, & J. J. E. Hayes, *PASP Conf Ser.*, 77, 398
- Villalobos A., & Helmi A. 2008, *MNRAS*, 391, 1806
- Zacharias, N., Urban, S. E., Zacharias, M. I., et al. 2004, *AJ*, 127, 3043
- Yanny, B., Rockosi, C., Newberg, H. J., et al. 2009, *AJ*, 137, 4377
- Zhao, G., Zhao, Y.-H., Chu, Y.-Q., Jing, Y.-P., & Deng, L.-C. 2012, *Res. Astron. Astrophys.*, 12, 723
- Zucker, D. B., de Silva, G., Freeman, K., Bland-Hawthorn, J., & Hermes Team 2012, *Galactic Archaeology: Near-Field Cosmology and the Formation of the Milky Way*, eds. M. Aoki, M. Ishigahi, T. Suda, T. Tsujimoto, & N. Asimoto, *ASP Conf. Proc.*, 458, 421